Journal of Hazardous Materials 169 (2009) 318–323

Contents lists available at ScienceDirect

Journal of Hazardous Materials

journal homepage: www.elsevier.com/locate/jhazmat

Removal and recovery of acridine orange from solutions by use of magnetic nanoparticles

Shahnaz Qadri, Ashley Ganoe, Yousef Haik*

Center of Research Excellence in Nanobiosciences, University of North Carolina at Greensboro, 321 McIver Street, 203 Eberhart Building, Greensboro, NC 27402, United States

ARTICLE INFO

Article history:
Received 16 July 2008
Received in revised form 16 March 2009
Accepted 21 March 2009
Available online 31 March 2009

Keywords:
Acridine orange
Nanoparticles
Magnetic
Dye recovery

ABSTRACT

Here we report a separation of a cationic dye, acridine orange (AO), by use of magnetic nanoparticles (γ-Fe_2O_3). The particles were showed to capture 98% of the dye within the first 20 min of contact time. The maximum sorption capacity of the magnetic nanoparticles (MNPs) for AO was 59 mg/g. The sorption isotherms fit well with the Freundlich model. The sorption kinetics fits well the pseudo-second-order rate equation model. 60–90% dye recovery was achieved by rotary evaporating the dye bearing nanoparticles in acetone. The nanoparticles were recycled for additional dye removal.

1. Introduction

Many of the industrial dyes are toxic, carcinogenic, mutagenic and teratogenic [1–3]. Their removal from wastewater is of great interest. Due to their stable behavior under harsh condition and resistance to biodegradation, non-conventional methods of wastewater treatments are explored [4,5]. Adsorption techniques by use of activated carbon are the most reported in the literature. However, due to its cost and low recyclability of the sorbent, activated carbon sorbents are losing interest [6–10].

Low cost dye removal based on natural byproducts such as coconut husk, banana pith, sunflower stalks, corncob, barley husk, rice husk, lemon peel, peanut hull and soybean hull have reported [11–18]. Some of these natural byproducts have been further chemically modified to enhance their sorption ability [19,20]. Besides byproducts, sand and clay has also been reported for dye adsorption [21,22].

Little work has been reported on the use of magnetic particles to remove toxic dye from wastewater. Magnetic separation has found great applications in biological species separation [23–27]. The magnetic separation provide suitable route for online separation, where particles with affinity to target species are mixed with the heterogeneous solution. Upon mixing with the solution, the particles tag the target species. External magnetic fields are then applied to separate the tagged particles from the solution. Qu et al. [28] filled multiwall carbon nanotubes with iron oxides and were able to demonstrate dye removal from aqueous solution. Preparation of the CNT–FeO complex may pose a limitation of this technique in industrial settings. Little work has been reported in the recovery of dye after removal from wastewater.

Acridine orange (AO), a cationic dye, has been the subject of extensive studies in recent years. The biological effects of AO, which includes photodynamic and mutagenic actions of the dye, constitute another large area of research [29,30].

In this work, nanoparticles made of Fe_2O_3, are utilized for removal of a cationic dye, acridine orange, from aqueous solution. The surface area to volume ratio for the nanoparticles lends an advantage in the separation of dyes. The sorption kinetics of AO into the γ-Fe_2O_3 nanoparticles is investigated. Additionally, a recovery technique of the dye from the nanoparticles using suspension and evaporation in acetone is also described.

2. Experimental

2.1. Materials and methods

Ferrous chloride hepta hydrate, ferric chloride tetra hydrate, sodium hydroxide, nitric acid, AO are all obtained from Sigma Chemical Company and used as such.

The preparation of iron oxide nanoparticles was done mainly in three steps.

(1) Co-precipitation of ferrous chloride hepta hydrate and ferric chloride tetra hydrate by sodium hydroxide:ferrous chloride

* Corresponding author. Tel.: +1 336 334 4625; fax: +1 336 334 8797.
E-mail address: y_haik@uncg.edu (Y. Haik).

0304-3894/$ – see front matter © 2009 Elsevier B.V. All rights reserved.
doi:10.1016/j.jhazmat.2009.03.103

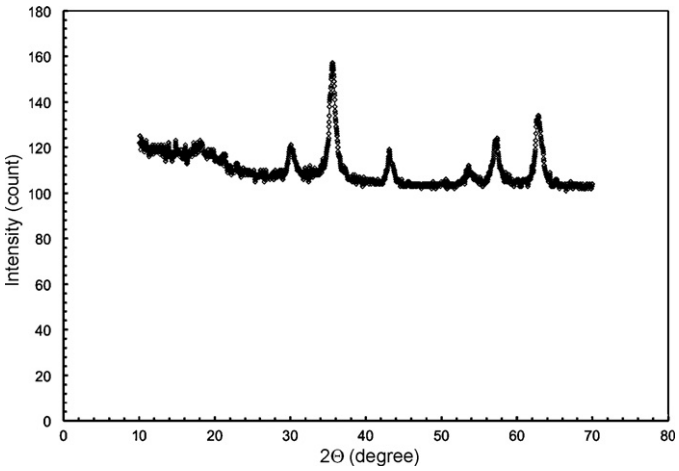

Fig. 1. Wide angle X-ray diffractogram for commercial and synthesized maghemite.

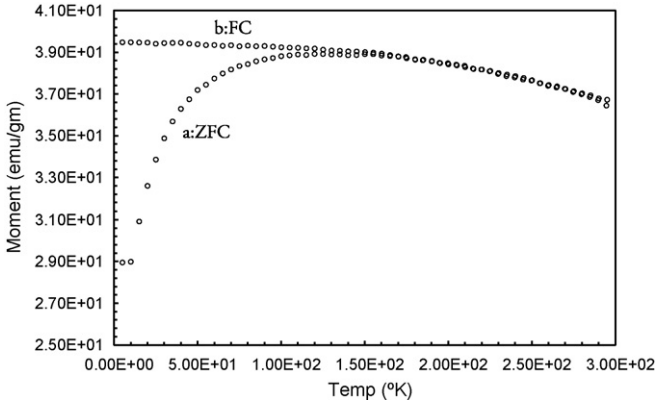

Fig. 3. Temperature–moment plot for synthesized maghemite.

and ferric chloride were mixed in a molar ratio of 1:2 in deionized water at a concentration of 0.1 M iron ions. The solution was used immediately after preparation. A highly concentrated solution of sodium hydroxide (10 M) was added to it for co-precipitation with continuous stirring.

(2) Heating and sonication: solution with the precipitate was stirred in high speed for 1 h at 20 °C then it was heated at 90 °C for 1 h with continuous stirring. The iron oxide dispersion was then sonicated for 10 min at 50% amplitude using a Cole Parmer Ultrasonic Homogenizer.

(3) Peptization with nitric acid: ultrafine magnetic particles obtained were peptized by nitric acid (2 M). The precipitate was then washed repeatedly with deionized water and filtered and dried in a vacuum to obtain fine iron oxide particles.

The X-ray diffraction pattern was obtained for the iron oxide particles to determine its crystalline phase (Philips wide angle X-ray diffractogram). Fig. 1 shows the wide angle X-ray diffractogram for the synthesized iron oxide particles. The particles are γ-Fe_2O_3 and crystalline in nature.

The particle size and shape of iron oxide was determined by transmission electron microscopy (TEM). 1 ml of suspension of particles was placed on carbon coated copper grids and observed under a scanning transmission electron microscope (JEOL STEM) at 200 kV. Electron micrographs and X-ray diffraction pattern were obtained with this microscope. Fig. 2 shows the TEM for the synthesized particles obtained at magnification of 500K. The particle has narrow distribution with average particles diameter of 9 ± 2.5 nm. The particles' size distribution was statistically obtained from a sequence of TEM images obtained at different magnifications analyzed by an image processing software (Digital Micrograph).

Magnetization measurements were performed using a superconducting quantum interference device (SQUID) magnetometer with a helium flow cryostat. Weighed amount of samples are packed in gel capsules and placed tightly in the glass tube ensuring no movement in either direction. Fig. 3 shows temperature dependence of magnetic moment for the synthesized sample on warming after (a) cooling in zero field (ZFC) and (b) cooling in an applied field of 50 G. The variation of temperature at which ZFC and FC separates (T_{sep}) was at 235 K and the maxima (T_B) was at 75 K.

Magnetization plots as a function of magnetic field is shown in Fig. 4 at both 5 K and at 300 K. The blocking temperature for the sample was about 75 K, which was below room temperature. Below the blocking temperature, particle showed ferrimagnetic behavior however at room temperature the sample exhibits superparamagnetic behavior.

Zeta potential for the particles was measured using a Malvern Zetasizer Nano ZS (Malvern Instruments Ltd.). Fig. 5 shows the zeta potential and ionic strength obtained for the maghemite particles.

AO with maximum absorption at 490 nm was obtained from Sigma Chemicals in commercial purity. Dye stock solutions 10^{-3} M were prepared and diluted to different initial concentrations for dye removal and recovery experiments. Fig. 6 shows the zeta potential and cationic strength of the AO.

Initial concentrations of dye solution were prepared in deionized water to ascertain the working concentration in Lambert–Beer range. Nanoparticles were used as dry weight in 1 mg, 2.5 mg, 5 mg and 7.5 mg and were suspended in 1 ml of deionized water. Stock

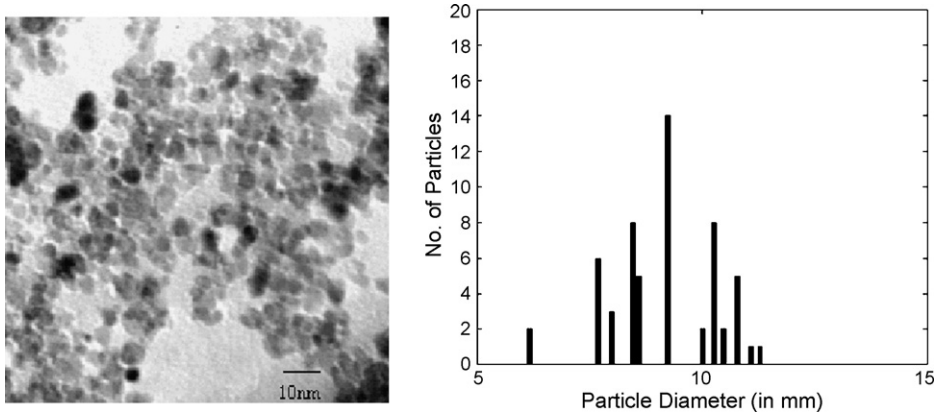

Fig. 2. TEM monograph and particle distribution of the synthesized particles.

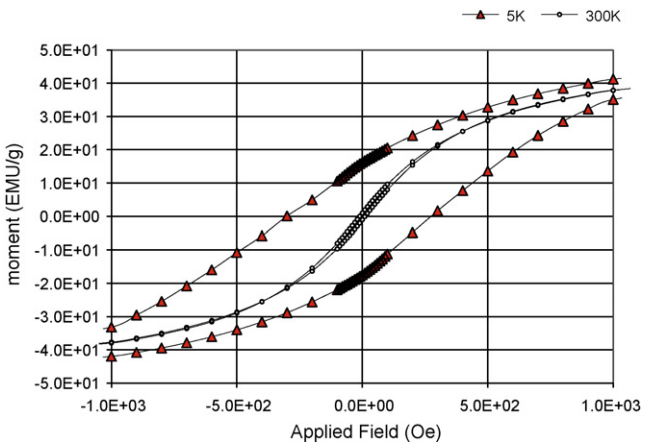

Fig. 4. Applied field versus magnetization plot of synthesized maghemite.

solution of dye was 10^{-3} M was prepared in 50 ml of deionized water.

3. Results and discussion

3.1. Equilibrium studies

Dye removal experiments were carried out by adding fixed amount of maghemite nanoparticles 5 mg/ml into a 15 ml falcon tube with a definite volume of 10 ml each with different dye concentrations ranging between 5×10^{-4} M and 1×10^{-5} M at room temperature 24 °C without changing the pH 4.5 ± 0.3, and inversely by keeping the dye concentration constant 5×10^{-4} M by adding the dry weight of nanoparticles in a range of 1–7.5 mg/ml in affixed volume of 10 ml. Followed by shaking on a shaker at 200 RPM to ensure equilibrium is reached. The tubes were sealed during the experiment to prevent evaporation and change in volume. At time $t = 0$, and equilibrium, dye concentrations were measured by double beam spectrum by UV–vis spectrophotometer at 490 nm. The

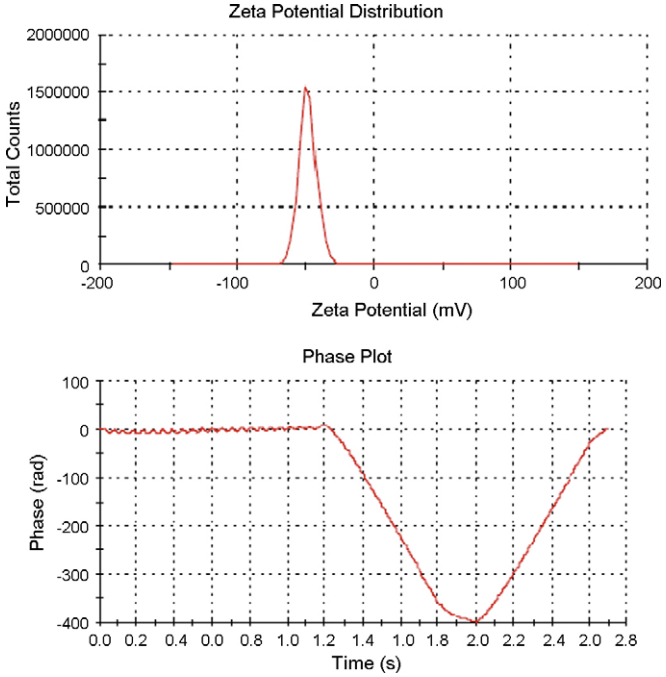

Fig. 5. Zeta potential and ionic strength of the maghamite particles.

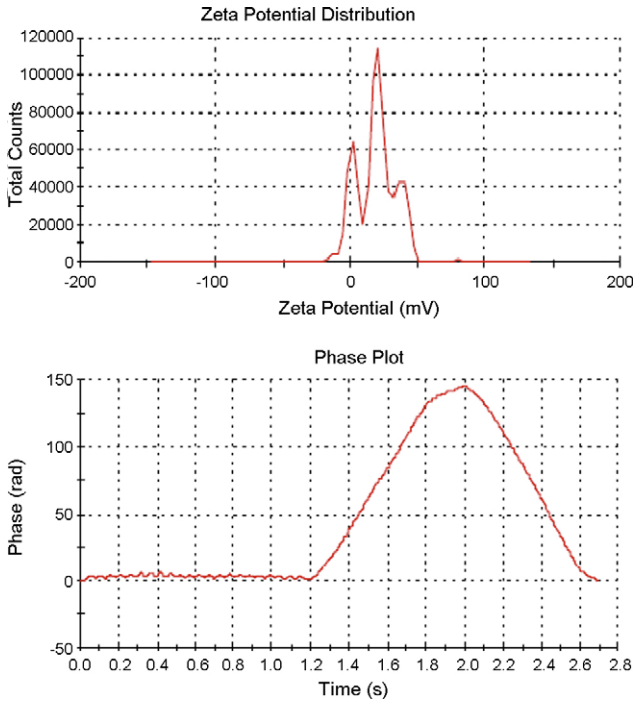

Fig. 6. Zeta potential and ionic strength of cationic AO.

amount of adsorption at equilibrium, q_t (mg/g) and was calculated by:

$$q_t = \frac{[C_0 - C_t]V}{W} \quad (1)$$

where C_0 and C_t (mg/L) are the liquid-phase concentrations of dye at initial and equilibrium after time (t) of incubation, respectively, V is the volume of the solution (L) and W is the mass of dry nanoparticles used (g).

After shaking for predetermined time intervals, the magnetic particles were separated magnetically. To ensure full isolation of the supernatant, the tubes were centrifuged for 5 min at 2000 rpm. The dye concentration in the supernatant was measured by UV–vis spectrophotometer at 490 nm. The experiments were conducted in duplicates and a positive (dye concentration at time $t = 0$) and negative (water) control were used to ensure accuracy of the spectral readings.

Fig. 7 shows the adsorption of AO on magnetic nanoparticles at different initial concentrations. In order to determine the equilibrium time, the adsorption of AO on magnetic particles was studied as function of contact time. It can be observed that the dye adsorption increases with the increase of concentration and time and at

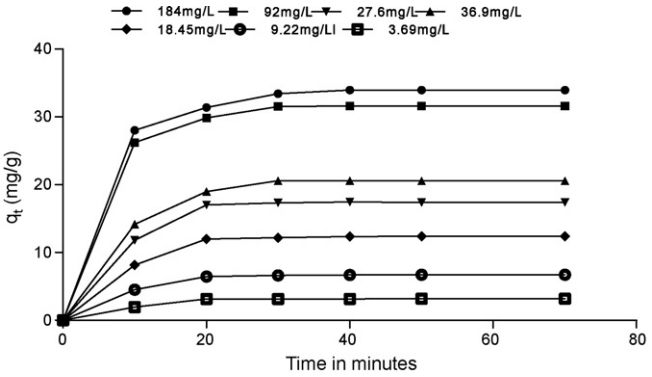

Fig. 7. Adsorption equilibrium results.

some point the adsorption remains constant where no more dye to remove. The equilibrium time to attain the maximum dye removal is detected in Fig. 7.

Fig. 7 also shows that as the initial dye concentration increases the amount of dye adsorbed also increases. It was obvious that the removal of dye was dependent on the concentration of dye. The amount of AO adsorbed increased from 3.6 mg/g to 35 mg/g as the concentration of dye was increased from 3.69 mg/L to 184 mg/L and nanoparticles was fixed as 5 mg.

Both the Langmuir and Freundlich equations were employed to study the sorption isotherms of AO. In the Langmuir equation

$$\frac{C_e}{q_e} = \frac{1}{Q_m a} + \frac{1}{Q_m} C_e \quad (2)$$

C_e is the concentration of the dye at equilibrium, q_e is the amount of sorbed dye at equilibrium. $C_e Q_m$ is the maximum sorption capacity and is the slope of the line formed when plotting C_e/q_e versus C_e. In the concentration range studied, Q_m was found to be 59.17 mg/g. In the C_e Freundlich equation.

$$q_e = kC_e^{1/n} \quad (3)$$

K and $1/n$ are empirical constants and their values are obtained by plotting $\ln(q_e)$ versus $\ln(C_e)$, where $\ln(K)$ is the intercept and $1/n$ is the slope of the line formed. The results indicated that the sorption isotherms of AO followed the Freundlich model better than the Langmuir model, with the following empirical relation (correlation coefficient of 0.956).

$$q_e = 2.43C_e^{1.5} \quad (4)$$

The sorption kinetics for all initial dye concentrations were treated with Ho's pseudo-second-order rate equation

$$\frac{t}{q_t} = \frac{1}{kq_e^2} + \frac{1}{q_e} \quad (5)$$

where q_t is the sorbed dye at time t, while q_e is the sorbed dye at equilibrium. Fig. 8 shows the results for all initial dye concentrations. Notably the initial absorption was fairly rapid and the pseudo equilibrium was reached after 20 min of contact time.

The pseudo-second-order rate equation constants for all of the initial concentrations used in the experiments are shown in Table 1.

The magnetic nanoparticles utilized in the experiment were 5 mg. Clearly the equilibrium sorption decreases as the dye concentration decreases. This is due to the availability of particles with unoccupied sites. As shown in Fig. 8, the experimental data fits well with the pseudo-second-order rate kinetic model.

3.2. Dye removal

The dye removal percentage can be calculated as follows:

$$\%\,Removal = \frac{C_0 - C_t}{C_0} \times 100 \quad (6)$$

where C_0 and C_t (mg/L) are the liquid-phase concentrations of dye at initial and equilibrium, respectively. The effects of agitation time and minimum adsorbent concentration upon the removal of AO dye at 24 °C are presented in Fig. 9. The amount of adsorbed dye in (mg/g) increased with increase in concentration of nanoparticles and agitation time, and remains nearly constant after equilibrium time. Hence, the higher initial concentration of adsorbent enhances the sorption process, and most of dye is adsorbed to achieve the equilibrium in about 20 min, although the data was measured for 70 min.

It should be highlighted that the major advantage that the magnetic separation offers is the ability to recover the dye from the nanoparticles and reticulate the particles for further dye separation. It also offers an online dye removal ability that lends itself well in industrial settings.

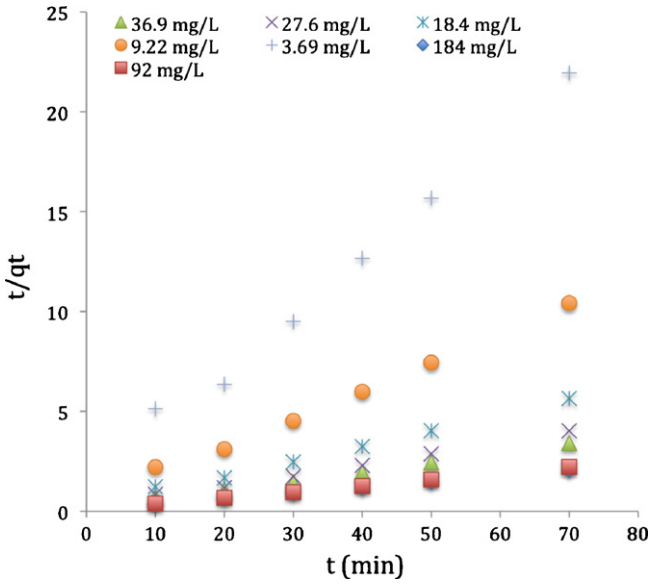

Fig. 8. Plot of t/q_t versus t for all of initial dye concentrations used in the experiments.

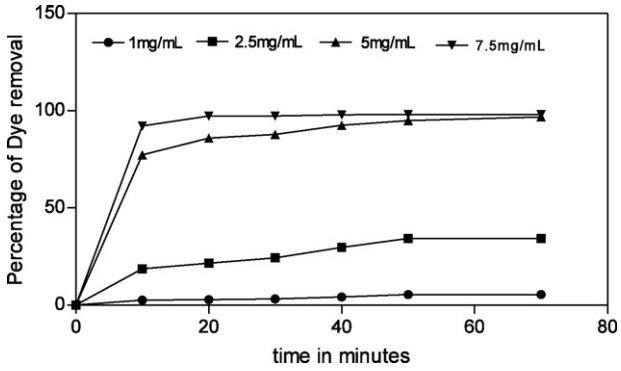

Fig. 9. Different concentrations of nanoparticles were taken as 1 mg/ml, 2.5 mg/ml, 5 mg/ml and 7.5 mg/ml with fixed dye concentration 5×10^{-4} M till equilibrium.

Table 1
Values of the pseudo-second-order rate equation constants.

Initial concentration (mg/L)	Equation	q_e (mg/g)	k (g/mg min)	R^2
184	$t/q_t = 0.0248t + 0.0609$	40.32	0.0101	0.99944
92	$t/q_t = 0.0306t + 0.0553$	32.68	0.0169	0.99937
36.9	$t/q_t = 0.0456t + 0.1627$	21.93	0.0128	0.99633
27.6	$t/q_t = 0.0542t + 0.1703$	18.45	0.0172	0.99502
18.45	$t/q_t = 0.0753t + 0.284$	13.28	0.0199	0.99491
9.22	$t/q_t = 0.1396t + 0.4959$	7.16	0.0393	0.99577
3.69	$t/q_t = 0.29t + 1.2471$	3.45	0.0674	0.99064

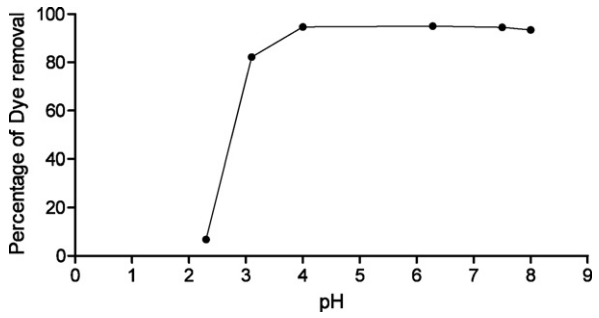

Fig. 10. Percentage of dye removal at different pH.

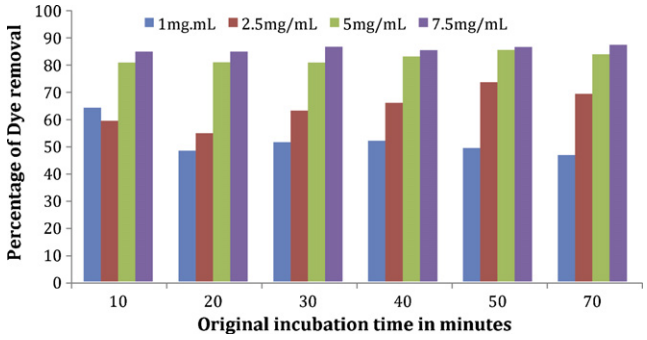

Fig. 11. Percentage of dye recovery.

The dye adsorption on sorbent was because of opposite charges between the sorbent and the dye. The adsorption of dye was influenced by change in pH. The effect of pH on the adsorption AO dye by the magnetic nanoparticles is presented in Fig. 10.

In this work dye concentration and magnetic nanoparticles concentration was fixed 5×10^{-4} M and 5 mg, respectively, in each in a final solution of 10 ml at 24 °C, the effect of pH was studied in a range 2.1–8. The solution pH would affect both aqueous chemistry and surface binding-sites of the adsorbent. The equilibrium sorption capacity was minimum at pH 2, which was 6.28% and increased up to pH 4.2 and reached maximum by 95% over the initial pH 4–7. At low pH, the H ions compete with dye, while at higher pH the magnetic nanoparticles have higher negative charge, which enhances the positively charged dye capturing through electrostatic force of attraction.

3.3. Dye recovery

Dye recovery from the nanoparticles was conducted by incubating the nanoparticles in acetone (cationic with four folds higher in charge than AO). Because of charge competition, the dye releases to acetone. The particles were collected magnetically from the acetone. The dye was recovered by rotary evaporating the acetone. The percentage of recovery was 60–90% depending on the amount of nanoparticles used. Fig. 11 shows the percentage of recovered dye. The magnetic particles were washed with deionized water and reused for dye removal.

4. Conclusions

Superparamagnetic nanoparticles with average size distribution of 9 ± 2.5 nm have been utilized for acridine orange dye removal and recovery from aqueous solution. The dye removal isotherms fit well with the Freundlich model. The kinetics of the dye removal fits well with the pseudo-second-order rate kinetic model. The maximum dye removal was 59 mg/g. Upon isolating the dye from the aqueous solution the magnetic particles carrying the dye were incubated in acetone. A maximum of 90% dye recovery was achieved following a dry evaporation of the acetone. The magnetic particles were washed and recycled for additional dye separation. The application of magnetic nanoparticles for dye removal and recovery provides a simple, but unique tool for industrial dye removal.

References

[1] H.A. Mekkawy, M.O. Ali, A.M. El-Zawahry, Toxic effect of synthetic and natural food dyes on renal and hepatic functions in rats, Toxicol. Lett. 95 (1998) 155–161.
[2] D.A. Oxspring, G. Mc Mullan, W.F. Smyth, R. Marchant, Decolourisation and metabolism of the reactive textile dye, Remazol Black B, by an immobilized microbial consortium, Biotechnol. Lett. 18 (1996) 527–530.
[3] E. Akceylan, et al., Removal efficiency of a calix[4]arene-based polymer for water-soluble carcinogenic direct azo dyes and aromatic amines, J. Hazard. Mater. 162 (2009) 960–966.
[4] S.R. Couto, Decolouration of industrial azo dyes by crude laccase from *Trametes hirsute*, J. Hazard. Mater. 148 (2007) 768–770.
[5] G.S. Nyanhongo, S.R. Couto, G.M. Guebitz, Coupling of 2,4,6-trinitrotoluene (TNT) metabolites onto humic monomers by a new laccase from *Trametes modesta*, Chemosphere 64 (2006) 359–370.
[6] K. Yang, X. Wang, L. Zhu, B. Xing, Competitive sorption of pyrene, phenanthrene, and naphthalene on multiwalled carbon nanotubes, Environ. Sci. Technol. 40 (2006) 5804–5810.
[7] A.W.M. Ip, J.P. Barford, G. McKay, Production and comparison of high surface area bamboo derived active carbons, Bioresour. Technol. 99 (2008) 8909–8916.
[8] A.E. Nemr, O. Abdelwahab, A. El-Sikaily, A. Khaled, Removal of direct blue-86 from aqueous solution by new activated carbon developed from orange peel, J. Hazard. Mater. 161 (2009) 102–110.
[9] A.G.E. Spantaleon, J.A. Nieto, M. Fernandez, A. Marsal, Use of activated clays in the removal of dyes and surfactants from tannery waste waters, Appl. Clay Sci. 24 (2003) 105–110.
[10] M.A.M. Khraisheh, M.S. Alg-Houti, Enhanced dye adsorption by microemulsion-modified calcined diatomite (mE-CD), Adsorption 11 (2005) 547–559.
[11] M.P. Elizalde-Gonzaĩez, A.A. Pelaĭez-Cid, Removal of textile dyes from aqueous solutions by adsorption on biodegradable wastes, Environ. Technol. 24 (2003) 821–829.
[12] I.A.W. Tan, A.L. Ahmad, B.H. Hameed, Adsorption of basic dye on high-surface-area activated carbon prepared from coconut husk: equilibrium, kinetic and thermodynamic studies, J. Hazard. Mater. 154 (2008) 337–346.
[13] M. Arami, N.Y. Limaee, N.M. Mahmoodi, N.S. Tabrizi, Removal of dyes from colored textile wastewater by orange peel adsorbent: equilibrium and kinetic studies, J. Colloid Interface Sci. 288 (2005) 371–376.
[14] O. Ozdemir, B. Armagan, M. Turan, S. Mehmet, Çeli, comparison of the adsorption characteristics of azo-reactive dyes on mesoporous minerals, Dyes Pigments 62 (2004) 49–60.
[15] R. Gong, Y. Sun, J. Chen, H. Liu, C. Yang, Effect of chemical modification on dye adsorption capacity of peanut hull, Dyes Pigments 67 (2005) 175–181.
[16] Y. Guo, J. Zhao, H. Zhang, S. Yang, J. Qi, Z. Wang, X. Hongding, Use of rice husk-based porous carbon for adsorption of Rhodamine B from aqueous solutions, Dyes Pigments 66 (2005) 123–128.
[17] R. Gong, M. Li, C. Yang, Y. Sun, J. Chen, Removal of cationic dyes from aqueous solution by adsorption on peanut hull, J. Hazard. Mater. 121 (2005) 247–250.
[18] T. Robinson, B. Chandran, P. Nigam, Removal of dyes from an artificial textile dye effluent by two agricultural waste residues, corncob and barley husk, Environ. Int. 28 (2002) 29–33.
[19] S. Senthilkumaar, P. Kalaamani, C.V. Subburaam, Liquid phase adsorption of crystal violet onto activated carbons derived from male flowers of coconut tree, J. Hazard. Mater. B136 (2006) 800–808.
[20] R. Gong, Y. Jin, J. Chen, Y. Hu, J. Sun, Removal of basic dyes from aqueous solution by sorption on phosphoric acid modified rice straw, Dyes Pigments 73 (2007) 332–337.
[21] M.A. Rauf, A.I. Shehadi, W.W. Hassan, Studies on the removal of Neutral Red on sand from aqueous solution and its kinetic behavior, Dyes Pigments 75 (2007) 723–726.
[22] M. Borisover, R.E. Graber, F. Bercovich, Z. Gerstl, Suitability of dye–clay complexes for removal of non-ionic organic compounds from aqueous solutions, Chemosphere 44 (2001) 1033–1040.
[23] C.H. Yu, K.Y. Tam, C.C.H. Lo, S.C. Tsang, Functionalized silica coated magnetic nanoparticles with biological species for magnetic separation, IEEE Trans. Magn. 43 (2007) 2436–2438.
[24] C.-J. Chen, Y. Haik, J. Chatterjee, Development in nanomagnetic Particles and biomedical applications, in: Recent Research Developments in Magnetism and Magnetic Materials, Transworld Research Network, Recent Research Development in Magnetism and Magnetic Materials, 2003.
[25] Y. Haik, J. Chatterjee, C.-J. Chen, Synthesis and stabilization of Fe–Nd–B nanoparticles by chemical Method, J. Nanopart. Res. 7 (2005) 675–679.
[26] R. Sharma, R.Y. Haik, C.-J. Chen, A search of superparamagnetic iron oxide-myoglobin as potential nanoparticle: iron oxide-myoglobin binding properties

and magnetic resonance image marker in mouse imaging, J. Exp. Nanosci. 2 (2007) 127–138.
[27] T. Lund-Olesen, H. Bruus, M.F. Hansen, Quantitative characterization of magnetic separators: comparison of systems with and without integrated microfluidic mixers, Biomed. Microdevices 9 (2007) 195–205.
[28] S. Qu, F. Huang, S. Yu, G. Chen, J. Kong, Magnetic removal of dyes from aqueous solution using multi-walled carbon nanotubes filled with Fe_2O_3 particles, J. Hazard. Mater. 160 (2008) 643–647.
[29] A.A. Ogunjobi, O.E. Fagade, O.O. David, Antimutagenic and potential anticarcinohenic activities of aloe-vera gel and aqueous garlic extract in bacterial reserve mutation test, Afr. Biomed. Res. 10 (2007) 275–278.
[30] P.K. Saetzler, J. Jallo, H.A. Lehr, C.M. Phillips, U. Vasthare, K.E. Arfors, R.F. Tuma, Intravital fluorescence microscopy: impact of light induced phototoxicity on adhesion of fluorescently labeled leukocytes, J. Histochem. Cytochem. 45 (1996) 505–513.